Systems & Control Transactions

Original Research Article
Peer Reviewed Conference Proceeding
ESCAPE 36 - European Symposium on Computer Aided Process Engineering
Sheffield, UK. 21-24 June 2026

PSE PRESS

Modeling and Optimization of Sonochemical Reactors through simulations

Nikolaos I. Vittas[a], Antonios Armaou[ab*]

[a] Chemical Engineering Department, University of Patras, Patras 26504, Greece
[b] Chemical Engineering Department, The Pennsylvania State University, University Park 16802, PA, USA
* Corresponding Author: armaou@upatras.gr .

ABSTRACT

Sonochemical reactors are a promising technology in process intensification, offering a sustainable and energy-efficient means of enhancing chemical reactions. By harnessing acoustic cavitation – the formation, oscillation and violent collapse of bubbles in a liquid medium – these systems generate local hotspots that can accelerate reaction kinetics. Despite its potential, efficient design and scale-up of sonochemical reactors remain major challenges, mostly because the cavitation phenomena take place close to the ultrasonic transducer. This work presents a simulation-based framework for the optimization of sonochemical batch reactors by coupling microscopic-level bubble behavior with macroscopic-level reactor performance, focusing on the placement of transducers to maximize reaction activity.

Keywords: Batch Process, Modelling and Simulations, Optimization, Sonochemistry, Acoustic Cavitation

INTRODUCTION

Sonochemistry relies on the phenomenon of acoustic cavitation, i.e. the type of cavitation induced in a liquid medium by ultrasound or acoustic waves [1]. When such a wave propagates through a liquid it causes cavities (bubbles) to form, oscillate and finally collapse [2, 3]. During the rarefaction phase of the wave, cavities form and preexisting bubbles expand, while during the compression phase the bubbles contract. This oscillatory pattern continues until the prevailing conditions drive the bubble into a violent collapse. The result of this process is the creation of localized hotspots, characterized by extreme pressure and temperature, which in turn enhances chemical reactions.

For accurate modeling of sonochemical reactors, several physical phenomena must be considered in combination: wave propagation inside the liquid, bubble dynamics under the ultrasound, heat diffusion from the collapsing bubbles and reaction kinetics. The bubble dynamics were captured using the Keller–Miksis model, accounting for liquid compressibility, while the Helmholtz equation described wave propagation within the reactor, incorporating viscous, thermal, and acoustic damping. Reaction kinetics for the Fenton assisted degradation of cresols were modelled as a pseudo–first-order process governed by Arrhenius temperature dependence.

BUBBLE DYNAMICS

The dynamic oscillations of a single bubble in a liquid medium under the influence of applied ultrasound can be described based on the fundamental principles of force and energy equilibriums, which are employed to derive the Rayleigh-Plesset equation. Following this, the refinement suggested by Keller and Miksis will be presented to account for more complex phenomena and to provide a more accurate representation of the oscillations and collapse. Finally, the effect of multiple acoustic waves on single-bubble dynamics will be examined.

Force Equilibrium

A typical cavitation bubble, assumed to pre-exist in the liquid medium, consists of both vapor and gas. Consequently, the total pressure inside the bubble (p_{in}) is the sum of the vapor pressure (p_v) and the gas pressure (p_g).

$$p_{in} = p_v + p_g \tag{1}$$

The vapor pressure is assumed to remain constant, whereas the gas pressure undergoes significant changes and can be approximated as:

$$p_g V_b{}^k = constant \quad (2)$$

where $V_b = {}^4/_3 \pi R^3$ is the volume and R the radius of the bubble. The exponent k represents the heat capacity ratio and the specific value depends on the model approach and the material. In the case of an adiabatic process involving air, the ratio can approximately be:

$$k = \frac{C_p}{C_v} \cong 1.4 \quad (3)$$

For the bubble to expand by dR, the work required is $\sigma(8\pi R\, dR)$, where σ is the surface tension. Using the above definitions, the force equilibrium on the bubble wall can be expressed as:

$$p_{in}\,(4\pi R^2) = p_b(2\pi R^2) + \sigma(8\pi R) \quad (4)$$

where p_b is the pressure on the bubble wall.

It is assumed that the bubble is oscillating from an equilibrium point with radius R_0 and the static ambient pressure is $p_\infty = p_0$. Combining the above equations provides an expression for the pressure on the bubble wall.

$$p_b = \left(p_\infty + \frac{2\sigma}{R_0} - p_v\right)\left(\frac{R}{R_0}\right)^{3k} + p_v - \frac{2\sigma}{R} \quad (5)$$

The effect of the acoustic wave, represented as time dependent variable $p_s(t)$, is incorporated into the ambient pressure term

$$p_\infty = p_0 + p_s(t) \quad (6)$$

In most typical cases the pressure wave is sinusoidal with pressure amplitude of P_a and frequency f, superimposed on hydrodynamic pressure p_0:

$$p_s(t) = p_0 - P_a\ sin(2\pi f t) \quad (7)$$

Energy Equilibrium

The conservation of energy can be described as: the work of the oscillating bubble W_b, either positive for expansion or negative for contraction and collapse, must be equal to the work W_l plus kinetic energy E_k required by the liquid volume surrounding the cavity.

$$W_b = W_l + E_k \quad (8)$$

Each of these terms is calculated separately:

$$W_b = p_b \frac{4}{3}\pi\left(R^3(t) - {R_0}^3\right) \quad (9)$$

$$W_l = p_\infty \frac{4}{3}\pi\left(R^3(t) - {R_0}^3\right) \quad (10)$$

$$E_k = 2\pi\rho_L R^3(t)\left(\frac{dR(t)}{dt}\right)^2 \quad (11)$$

Rayleigh-Plesset

The combination of equations (5)-(11) yields the Rayleigh-Plesset equation, describing the radius of the bubble in respect to time.

$$\frac{3}{2}\left(\frac{dR(t)}{dt}\right)^2 + R(t)\frac{d^2R(t)}{dt^2} = \\ = \frac{1}{\rho_L}\left(p_g + p_v - \frac{2\sigma}{R(t)} - 4\mu\frac{1}{R(t)}\frac{dR(t)}{dt} - p_0 - p_s(t)\right) \quad (12)$$

Keller-Miksis

The Rayleigh – Plesset equation is foundational for any work done in acoustic cavitation. However, the main assumptions made, that the liquid is incompressible and the bubble remains spherical, are less than accurate for such high-speed phenomenon. To address these limitations, the suggested modifications by Keller and Miksis [4, 5] account mainly for the compressibility of the liquid, as well as effects of viscosity, surface tension and acoustic radiation

$$\left[1 - \frac{1}{3}(3\Lambda + 1)\frac{1}{c_L}\frac{dR(t)}{dt}\right]\frac{3}{2}\left(\frac{dR(t)}{dt}\right)^2 + \\ + \left[1 - (\Lambda + 1)\frac{1}{c_L}\frac{dR(t)}{dt}\right]R(t)\frac{d^2R(t)}{dt^2} = \\ = \left[1 + (1 - \Lambda)\frac{1}{c_L}\frac{dR(t)}{dt} + \frac{R}{c_L}\frac{d}{dt}\right]\frac{p_b - p_\infty}{\rho_L} \quad (12)$$

In the present work the parameter $\Lambda = 0$, referring to the Keller form of the equation.

Collapse

The analysis of the transient collapse of the oscillating gas filled cavity [6] assumes that the bubble reaches a maximum radius R_{max} just before the violent collapse to a minimum radius $R_{min} \to 0$. The collapse is characterized by the bubble wall reaching its maximum velocity under the assumption of adiabatic compression of the internal gas. As a result, the gas reaches exceedingly high pressures and temperatures during the collapse. The maximum temperature reached during the process can be determined, using the initial temperature T_0, by the following relationship [7].

$$T_{max} = T_0\left(\frac{R_{max}}{R_{min}}\right)^{3(\gamma-1)} \quad (13)$$

Different Wave Sources

A preliminary approach to analyze the effect of multiple wave sources on the single bubble dynamics can be made via simple modifications to the existing model. The equation (7) can be modified to account, for instance, two distinct waves characterized by amplitudes and frequences P_{a1}, f_1 and P_{a2}, f_2 respectively [8, 9].

$$p_s(t) = p_0 - P_{a1} sin(2\pi f_1 t) - P_{a2}\ sin(2\pi f_2 t) \quad (14)$$

WAVE PROPAGATION

Analyzing wave propagation in a liquid medium containing dispersed bubble population requires a comprehensive approach. One of the most important parameters

in the cavitation theory is the void fraction β. It accounts for the total volume occupied by cavities inside the control volume V:

$$\beta = \frac{4}{3}\pi R_0^3 n \tag{15}$$

where $n = {}^{N}/_{V}$ is bubble number density and R_0 is the equilibrium radius that all bubbles are assumed to have [10].

Mass Conservation

The conservation of mass for a mixture of liquid and dispersed bubbles is expressed as:

$$\frac{\partial \rho}{\partial t} + \boldsymbol{\nabla} \bullet (\rho \boldsymbol{v}) = 0 \tag{16}$$

where $\boldsymbol{v}$ is the velocity and ρ is the density of the mixture, based on the void fraction

$$\rho = \rho_L(1-\beta) + \rho_g\beta \cong \rho_L(1-\beta) \tag{17}$$

It is apparent that the mixture density approaches the liquid density ρ_L, since the gas density ρ_g is negligibly small.

Assuming (a) negligible bubble coalescence and fragmentation, (b) bubbles move at the same velocity as the liquid and (c) the void fraction is of the order of 10^{-4} or smaller, the equation for conservation of mass is:

$$\frac{1}{\rho_L}\frac{D\rho_L}{Dt} + \boldsymbol{\nabla} \bullet v = 4\pi R^2 \frac{DR}{Dt} \tag{18}$$

Energy Conservation

The momentum conservation is ensured via Cauchy relationship:

$$\rho_L\left[\frac{\partial v}{\partial t} + \boldsymbol{v} \bullet \boldsymbol{\nabla v}\right] = \boldsymbol{\nabla} \bullet \bar{\bar{\sigma}} + \boldsymbol{f} \tag{19}$$

Neglecting viscous terms expressed via the stress tensor $\bar{\bar{\sigma}}$ and the body forces given via $\boldsymbol{f}$ term, thereby considering only for pressure forces, the momentum conservation equation is simplified to:

$$\rho_L\left[\frac{\partial v}{\partial t} + \boldsymbol{v} \bullet \boldsymbol{\nabla v}\right] - \boldsymbol{\nabla} p = \boldsymbol{0} \tag{20}$$

Wave equation

The non-homogeneous wave equation can be derived through the nondimensionalization of the governing mass and momentum conservation equations. Following the work done by Calfisch and al. [11] the non-homogeneous wave equation can be obtained:

$$\frac{1}{{c_L}^2}\frac{\partial^2 p}{\partial t^2} - \nabla \bullet \nabla p - \frac{\partial^2 \beta}{\partial t^2} = 0 \tag{21}$$

It can be proven that the wave propagation in the bubbly liquid is following the Helmholtz's equation

$$\Delta P(t, \boldsymbol{r}) + {k_m}^2 P(t, \boldsymbol{r}) = 0 \tag{22}$$

where the complex wavenumber, a monodisperse bubble population with equilibrium radius R_0, for is defined by the relationship:

$${k_m}^2 = \frac{\omega^2}{{c_L}^2}\left(1 + 4\pi \frac{{c_L}^2 \frac{N}{V} R_0}{\omega_0 - \omega^2 + 2ib\omega}\right) \tag{22}$$

The wave number incorporates variables like resonance frequency (ω_0), damping constant (b) that accounts for viscous, thermal and acoustic effects and velocity potential (Φ) given by the following relationships:

$$\omega_0 = \frac{p_0}{\rho_L {R_0}^2}\left[Re(\Phi) - \frac{2\sigma}{R_0 p_0}\right] \tag{23}$$

$$b = \frac{2\mu}{\rho_L {R_0}^2} + \frac{p_0}{2\rho_L {R_0}^2} Im(\Phi) + \frac{\omega^2 R_0}{2c_L} \tag{24}$$

$$\Phi = \frac{3\gamma}{1 - 3(\gamma-1)i\frac{Dg}{\omega {R_0}^2}\left[\sqrt{i\frac{\omega {R_0}^2}{Dg}}coth\left(\sqrt{i\frac{\omega {R_0}^2}{Dg}}\right) - 1\right]} \tag{25}$$

REACTION

Fenton oxidation is a promising method for the degradation of pollutants like phenols. In Fenton process, hydroxyl radicals OH^- are produced from hydrogen peroxide H_2O_2 catalyzed by iron Fe(II).

$$Fe^{2+} + H_2O_2 \rightarrow Fe^{3+} + OH^- + OH \bullet \tag{26}$$

The generated radicals can react effectively with a variety of organic compounds RH.

$$RH + OH \bullet \rightarrow H_2O + R \bullet \rightarrow \textit{further oxidation} \tag{27}$$

$$R \bullet + H_2O_2 \rightarrow ROH + OH \bullet \tag{28}$$

Batch Reactor

Considering a well-mixed mixture, two areas of interest can be assumed. The first one is where the cavitation takes place, which is essentially the part of the liquid that has elevated temperature due to a bubble collapse, thus an enhanced reaction rate. The second one is the rest of the bulk liquid having an ambient temperature, thus a base reaction rate. The areas are symbolized with c and B respectively. The mass equilibrium for a product with concentration, C, may then be written as:

$$\frac{dC}{dt} = \beta r_c + (1-\beta) r_B \tag{29}$$

where β is the void fraction and r the rate of the reaction.

Effective Rate

Although this theory may be applied to different reactions, this work focuses on the degradation of cresols, due to the reaction being well documented under a variety of conditions.

$$C_7H_8O + 17H_2O_2 \rightarrow 7CO_2 + 21H_2O \tag{30}$$

Assuming abundance of H_2O_2, a pseudo-first-order reaction rate for the organic compound is given by:

$$r = -kC \tag{31}$$

where the constant k has an Arrhenius dependency of temperature:

$$k = A\exp\left(\frac{E_A}{RT}\right) \quad (32)$$

In the bulk liquid with an ambient temperature T_0, the rate constant would be:

$$k_B = A\exp\left(\frac{E_A}{R_g T_0}\right) \quad (33)$$

While in the area affected by cavitation phenomena, heat diffusion in the surrounding liquid must be considered. Thus, the rate constant would be given by the following equation:

$$k_{eff} = \frac{\int_t \int_V k(t,\boldsymbol{r})dVdt}{\int_t \int_V dVdt} \quad (34)$$

By integrating Eq. (29) a more convenient variable for comparison can be derived, hereafter referred to as effective rate r_{eff}:

$$-ln\left[\frac{C}{C_0}\right] = \left[\beta k_{eff} + (1-\beta)k_B\right]t \quad (35)$$

where:

$$r_{eff} = \beta k_{eff} + (1-\beta)k_B \quad (36)$$

SIMULATION DETAILS

Geometry

The sonochemical reactor is a cylindrical batch reactor, open at the top, with a cylindrical transducer submerged from the top. The ultrasound is introduced into the system from the tip of the transducer.

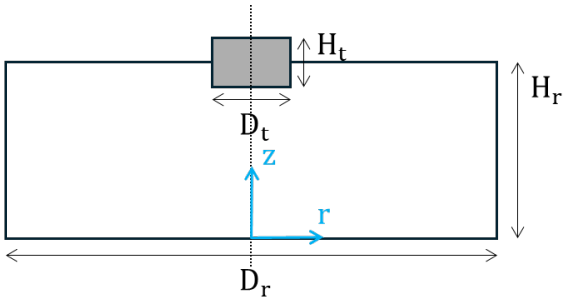

Figure 1. Geometric characteristics of the reactor.

The reactor is filled with an aquatic solution. The geometry of the reactor is described in Figure 1 and Table 1

Table 1. Geometrical characteristics of the reactor.

Symbol	Value
D_r	0.5 m
D_t	0.08 m
H_r	0.2 m
H_t	0.1 m

Parameters

The liquid medium is water at standard temperature and pressure, thus $T_0 = 298.15$ K and $p_0 = 1.01325 \cdot 10^5$ Pa. The physical properties of water are given in Table 2.

Table 2. Physical properties of water.

Symbol	Value
Γ	4/3
Σ	$0.0725\ \mathrm{N \cdot m^{-1}}$
M	$1.0016 \cdot 10^{-3}\ \mathrm{Pa \cdot s}$
ρ_L	$1000\ \mathrm{kg \cdot m^{-3}}$

The acoustic wave travels at the frequency of $f = 20$ kHz and with an amplitude that is calculated by the following relationship [8, 12]:

$$P_a = \sqrt{2\rho_L c\frac{P}{A_t}} \quad (37)$$

where P is the power of the transducer set to 40 W and $A_t = 0.005\ \mathrm{m^2}$ the area of the tip of the transducer. Thus, the amplitude of the wave is set to be $P_a = 1.53 \cdot 10^5$ Pa.

In terms of the reaction, for p-cresols the Arrhenius constants are $A = 0.1419\ \mathrm{s^{-1}}$ and $E_a = 14.25 \cdot 10^3\ \mathrm{J\ mol^{-1}}$.

It should be noted that equilibrium radius of the single bubble is considered to be $R_0 = 5\ \mu$m and the void fraction is calculated via the following empirical relationship [13]:

$$\beta = N \cdot |p| \quad (38)$$

where $N = 2 \cdot 10^{-9}$.

RESULTS

The results of the simulation can be divided into two categories: the single-bubble environment, which accounts for the enhancement of the reaction through an increase of the rate constant and wave propagation inside the batch reactor, which reflects the intensity of cavitation phenomena through an increase of the void fraction.

Single-Bubble Environment

The effect of one wave and two coherent waves on the single bubble have been simulated. Figures 2 and 3 demonstrate the radius changes for each case.

The bubble grows 15 and 50 times its equilibrium size respectively and then it rapidly collapses before the completion of on cycle. The temperature reached by the bubble during the collapse, based on the maximum radius the bubble reaches, is 4780 K for one wave and 13987 K for two waves. Applying a simple conduction model, the area effected by cavitation is 2 times the equilibrium radius and this effect is sustained for 10 periods for both cases.

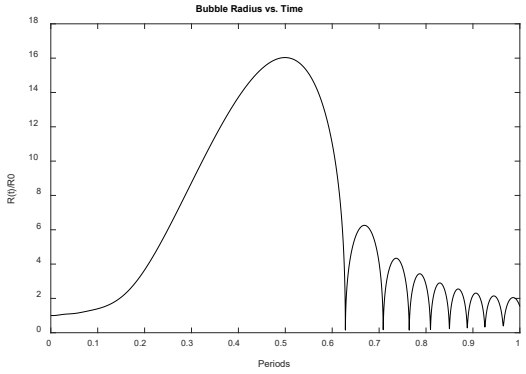

Figure 2. Bubble radius as a function of time under one acoustic wave.

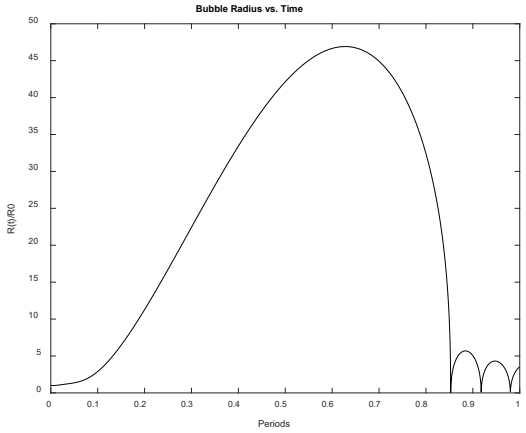

Figure 3. Bubble radius as a function of time under two identical acoustic waves

The rate constant in these conditions can be calculated to be $0.2788\ \mathrm{s}^{-1}$ and $0.7733\ \mathrm{s}^{-1}$ respectively, while in bulk conditions the constant is $4.5213 \cdot 10^{-4}\ \mathrm{s}^{-1}$. This accounts for an increase of 615% and 1700% for the rate constant in the cavitation zone compared to the bulk of the liquid.

One transducer

The first simulation examines a transducer placed at the center of the top of the reactor as shown in Figure 4.

The propagation of the wave in the liquid medium was described by the pressure distribution inside the reactor, while the void fraction demonstrated where cavitation phenomena occur. The YZ cut-plane of the reactor is presented for both parameters in Figures 5 and 6.

The pressure wave appears to have an effect mostly close to the transducer, although small pressure variations exist everywhere inside the reactor. The higher void fraction, in the order of $9 \cdot 10^{-4}$, exists just under the transducer. The mean void fraction was calculated to be $5.32 \cdot 10^{-5}$.

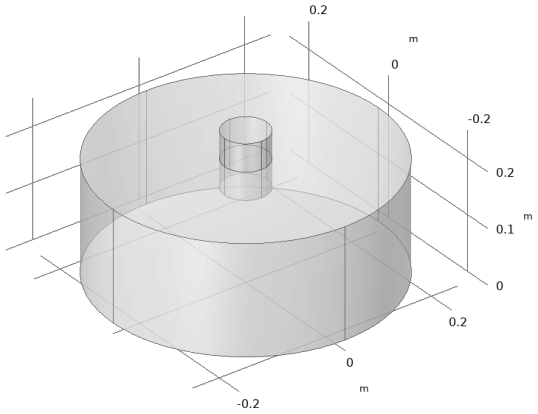

Figure 4. Geometry of one transducer at the center of the top of the reactor.

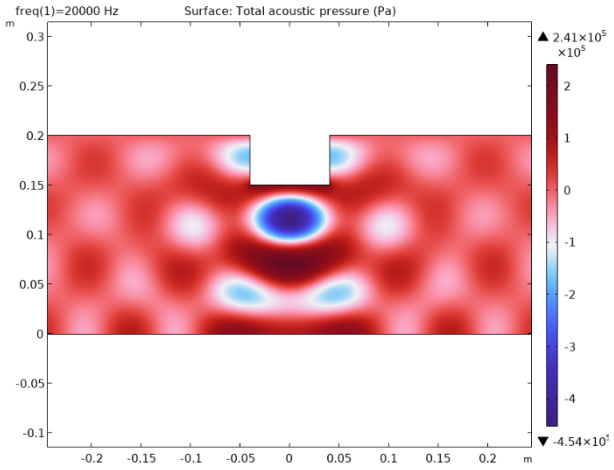

Figure 5. Pressure distribution for one transducer.

Given this result and the rate constant for one wave, the effective rate was calculated to be $4.648 \cdot 10^{-4}\ s^{-1}$. This is an increase of 2.8% in the reactions rate. Literature data suggest that the rate is around $4.5 \cdot 10^{-4} s^{-1}$, depending on the exact conditions [14, 15].

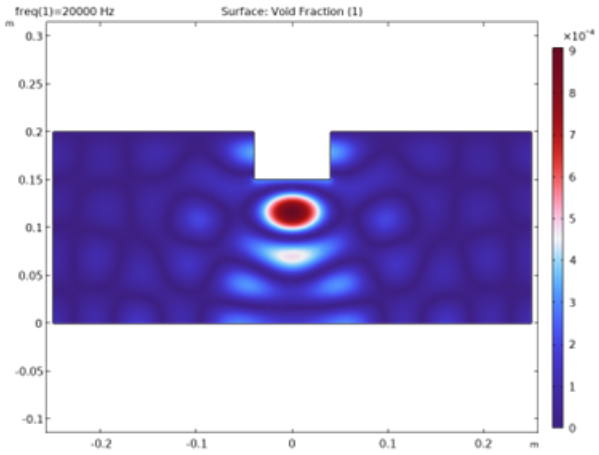

Figure 6. Void fraction for one transducer.

Two transducers

The simplest geometry to simulate the wave propagation from two different transducers is one at the center top of the reactor (as before) and the other at the center bottom of the reactor. Note that for practical reasons the tip of the bottom transducer is placed on the same plane as the bottom of the reactor.

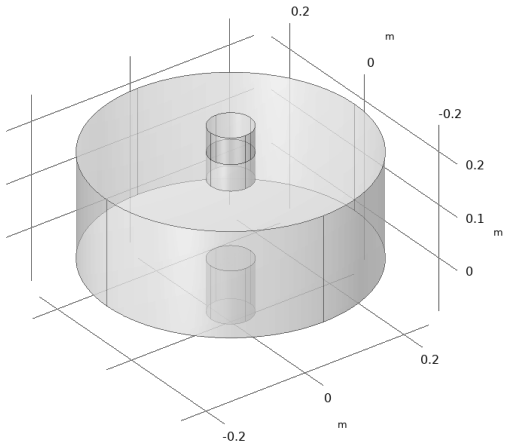

Figure 7. Geometry for two transducers.

The same YZ-plane plots for the pressure and void fraction distributions are presented in Figures 8 and 9 respectively. Both figures show little to no changes for the addition of another transducer, just a slightly increased intensity of the variations in the central axis. The mean void fraction was calculated as $4.82 \bullet 10^{-5}$, lower than previously.

Despite that, the two waves introduced into the system affect the single bubble dynamics differently, resulting in more extreme phenomena. Thus, the effective rate was calculated to be $4.873 \bullet 10^{-4} s^{-1}$, representing a 4.8% increase compared to the one transducer simulation.

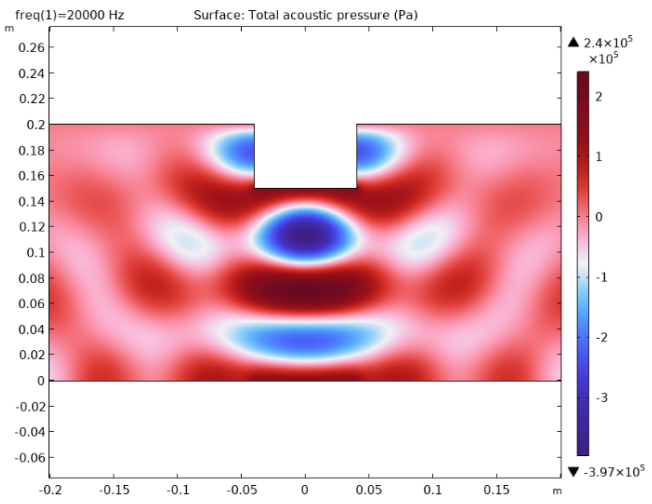

Figure 8. Pressure distribution for two transducers

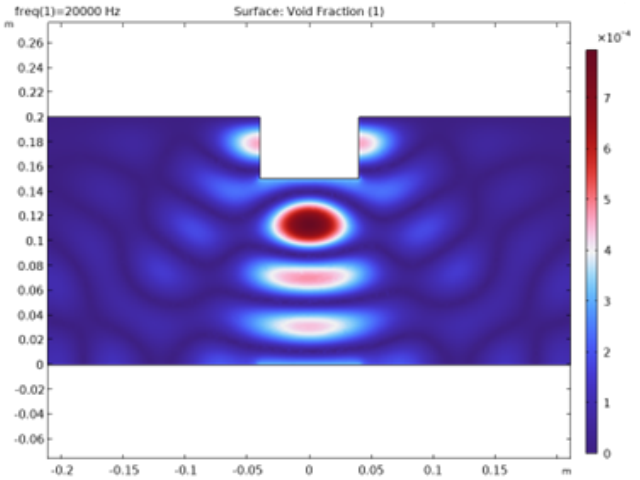

Figure 9. Void fraction for two transducers.

Optimization

To maximize the effective rate we investigated changing the position of the top transducer in all directions and the bottom transducer in x and y directions.

The optimum configuration was found to involve both transducers positioned at the center of the reactor, with the top transducer submerged as deeply as possible. The maximum effective rate was calculated to be $5.640 \bullet 10^{-4} s^{-1}$, which accounts for an increase of 15.7% of the rate calculated in the simple simulation.

In this case, the results were verified by the wave propagation as well. As shown in Figure 10, the pressure distribution changed drastically, when the transducer was well placed. On the central axis, the combination of the two transducers resulted in higher pressure amplitude. Due to more efficient reflection on the walls, the phenomenon was spreading to the rest of the bulk liquid, since pressure variations are observed in all the reactor.

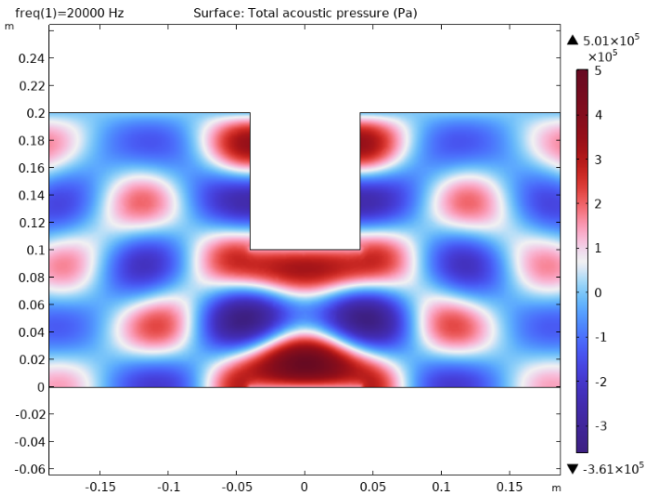

Figure 10. Pressure distribution for optimal position for the transducers.

The Void fraction mapping presented in Figure 11 further clarifies the result. Not only the areas with high void fraction were increased between the transducers, but the value of void fraction within these areas was increased as well. The mean void fraction was calculated to be $1.475 \cdot 10^{-4}$, an increase of 206%.

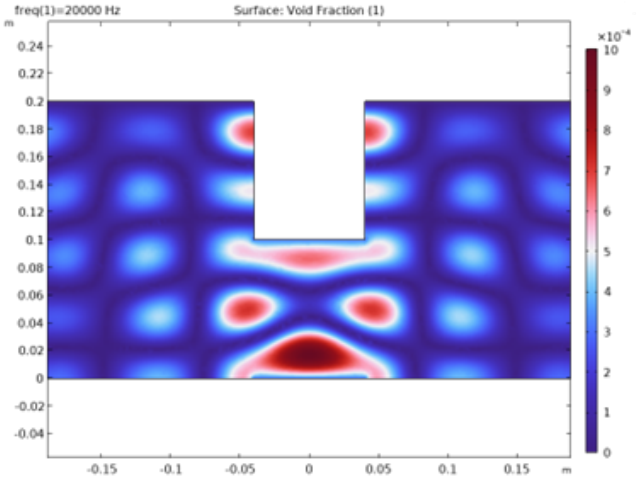

Figure 11. Void fraction for optimally positioned transducers.

It should be noted that the void fraction depends on the total volume of the liquid. Submerging the transducer more into the liquid, lowers the liquid volume, resulting in an increase of the void fraction. This plays an important role in the increase and should be expected. Furthermore, the fact that both transducers were optimally placed along the central axis rather than near the walls indicates that, for the present geometry characteristics, the most effective wave propagation occurs at the center, where the reflections constructively reinforce the acoustic field. In this arrangement, the pressure pulsations were symmetrically distributed throughout the reactor volume, ensuring that cavitation activity was present across most of the liquid domain.

Side transducers

Considering the optimization simulations performed up to this stage, the simulation of the side transducer was omitted, since the behavior of the effective rate was already established. The subsequent step was to determine the optimal placement along the z direction.

The optimal position was found to be in about ¾ the height of the reactor. The mean void fraction and the effective rate of the reaction were calculated to be $8.828 \cdot 10^{-5}$ and $4.746 \cdot 10^{-4}\ s^{-1}$ respectively. This was a slight improvement over only one transducer present.

The intuitive position for the transducer would probably be at half of the height of the reactor for symmetry or as low as possible to enable strong reflection from the walls. However, the optimum position was not even close to these, proving the complexity of wave propagation inside the reactor.

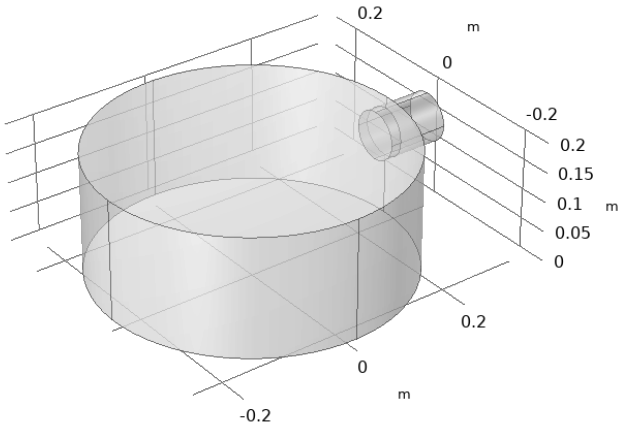

Figure 12. Optimal position for one side transducer.

Since the optimal height for one transducer had been calculated, the next optimization was focused on a second side transducer and its relative position to the first one. The optimal position is shown in Figure 13.

The mean void fraction was found to be $1.216 \cdot 10^{-4}$, while the rate of the reaction was $5.440 \cdot 10^{-4} s^{-1}$, which accounted for a 14.6% increase relative to just one transducer.

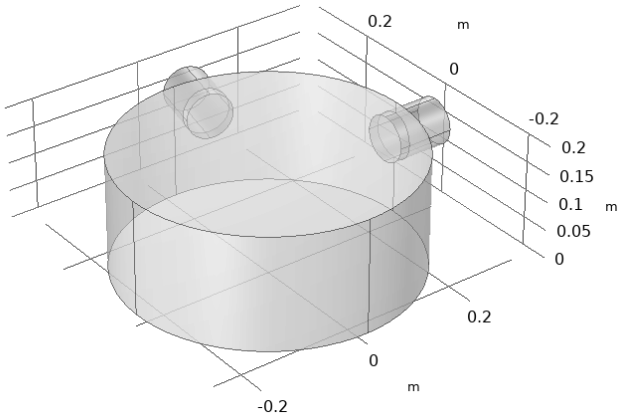

Figure 13. Optimal position for two side transducers.

It was expected that the optimum placement for the two side transducers would also be at the opposite sides of the reactor (like the vertical positioning problem solution). However, the optimization results indicates that this is not the case. This outcome can be attributed either to the horizontal orientation of the transducers that change drastically the wave propagation, or the fact that in the opposite-side configuration their separation distance is larger than in the vertical arrangement, increasing the wave damping throughout the liquid.

CONCLUSION

The present study examined the enhancement of batch reactor performance through the optimal placement of one or more ultrasonic transducers to increase chemical reaction rates. This objective was addressed through an optimization formulation incorporating multiscale modeling, integrating cavitation theory, wave propagation, heat diffusion, and reaction kinetics into a batch reactor model equipped with one or two transducers. Particular emphasis was placed on capturing the effect of transducer placement on reactor performance.

At the single-bubble scale, simulations showed that a bubble exposed to a single ultrasonic wave reached a collapse temperature of ~4800 K, whereas the interaction of two identical waves could increase the collapse temperature to 15, 000 K. This increase in temperature produced a substantial kinetic enhancement, with the reaction rate within the cavitation-affected volume increasing by 600% in the single-wave case and by 1700% in the two-wave case relative to nominal conditions.

At the reactor scale, a configuration with a single transducer submerged from the open top was used to establish baseline conditions. Cavitation activity, quantified by the void fraction, was concentrated beneath the transducer and provided reference values for both the mean void fraction and the effective reaction rate. The introduction of a second transducer increased the effective reaction rate by 5%, despite a slight decrease in the mean void fraction. This result indicates that reactor performance is governed not only by macroscopic wave propagation, but also by microscopic bubble dynamics.

The optimal placement of the two transducers was found to be along the central axis on opposite sides of the reactor, with the upper transducer submerged as deeply as possible. Under these conditions, the effective reaction rate was maximized, reaching a value 16% higher than that of the baseline configuration. Placing a single transducer on the reactor sidewall, had no significant performance enhancement. However, the addition of a second sidewall transducer at an optimized location increased the effective reaction rate by approximately 15% relative to the single-side configuration.

These findings demonstrate that simulation-based optimization can significantly improve the efficiency of sonochemical reactors by guiding the spatial arrangement of transducers. The proposed study highlights the potential of computational approaches for the rational design and scale-up of high-performance ultrasonic systems for chemical engineering applications.

AUTHOR IDENTIFIERS

Author ORCIDs:
Nikolaos Vittas:
Antonios Armaou: 000-0002-8592-7934

REFERENCES

1. Shah YT, Pandit AB, Moholkar VS. Cavitation reactors. The Plenum Chemical Engineering Series :193-245 (1999). https://doi.org/10.1007/978-1-4615-4787-7_6
2. Suslick KS. The chemical effects of ultrasound. Sci Am 260:80-86 (1989). https://doi.org/10.1038/scientificamerican0289-80
3. Kentish S, Ashokkumar M. Ultrasonic membrane processing. Food Engineering Series :583-598 (2010). https://doi.org/10.1007/978-1-4419-7472-3_23
4. Keller JB, Miksis M. Bubble oscillations of large amplitude. The Journal of the Acoustical Society of America 68:628-633 (1980). https://doi.org/10.1121/1.384720
5. A. Prosperetti and A. Lezzi, "Bubble dynamic in a compressible liquid. Part 1. First-order theory, " Fluid Mech., vol. 168, pp. 457-478, 1986.
6. Neppiras EA. Acoustic cavitation. Physics Reports 61:159-251 (1980). https://doi.org/10.1016/0370-1573(80)90115-5
7. Merouani S, Hamdaoui O, Rezgui Y, Guemini M. Theoretical estimation of the temperature and pressure within collapsing acoustical bubbles. Ultrasonics Sonochemistry 21:53-59 (2014). https://doi.org/10.1016/j.ultsonch.2013.05.008
8. Tatake PA, Pandit AB. Modelling and experimental investigation into cavity dynamics and cavitational yield: influence of dual frequency ultrasound sources. Chemical Engineering Science 57:4987-4995 (2002). https://doi.org/10.1016/s0009-2509(02)00271-3
9. Prabhu AV, Gogate PR, Pandit AB. Optimization of multiple-frequency sonochemical reactors. Chemical Engineering Science 59:4991-4998 (2004). https://doi.org/10.1016/j.ces.2004.09.033
10. Commander KW, Prosperetti A. Linear pressure waves in bubbly liquids: comparison between theory and experiments. The Journal of the Acoustical Society of America 85:732-746 (1989). https://doi.org/10.1121/1.397599
11. R. Caflish, M. Miksis, G. Papanicolaou and L. Ting, "Effective equations for wave propagation in bubbly liquids, " Fluid Mech., vol. 153, pp. 259-273, 1985.
12. Kanthale PM, Gogate PR, Pandit AB. Modeling aspects of dual frequency sonochemical reactors. Chemical Engineering Journal 127:71-79 (2007). https://doi.org/10.1016/j.cej.2006.09.023
13. Tiong TJ, Chu JK, Tan KW. Advancements in acoustic cavitation modelling: progress, challenges,

and future directions in sonochemical reactor design. Ultrasonics Sonochemistry 112:107163 (2025). https://doi.org/10.1016/j.ultsonch.2024.107163
14. Kavitha V, Palanivelu K. Destruction of cresols by fenton oxidation process. Water Research 39:3062-3072 (2005). https://doi.org/10.1016/j.watres.2005.05.011
15. Okouchi S, Nojima O, Arai T. Cavitation-induced degradation of phenol by ultrasound. Water Science and Technology 26:2053-2056 (1992). https://doi.org/10.2166/wst.1992.0659